Oncogene
https://doi.org/10.1038/s41388-020-1156-0

ARTICLE

Stabilization of FASN by ACAT1-mediated GNPAT acetylation promotes lipid metabolism and hepatocarcinogenesis

Li Gu[1,2] · Yahui Zhu[1,2] · Xi Lin[1,2] · Xingyu Tan[1,2] · Bingjun Lu[1,2] · Youjun Li[1,2]

Received: 18 April 2019 / Revised: 24 December 2019 / Accepted: 10 January 2020
© The Author(s), under exclusive licence to Springer Nature Limited 2020

Abstract

Metabolic alteration for adaptation of the local environment has been recognized as a hallmark of cancer. GNPAT dysregulation has been implicated in hepatocellular carcinoma (HCC). However, the precise posttranslational regulation of GNPAT is still undiscovered. Here we show that ACAT1 is upregulated in response to extra palmitic acid (PA). ACAT1 acetylates GNPAT at K128, which represses TRIM21-mediated GNPAT ubiquitination and degradation. Conversely, GNPAT deacetylation by SIRT4 antagonizes ACAT1's function. GNPAT represses TRIM21-mediated FASN degradation and promotes lipid metabolism. Furthermore, shRNA-mediated ACAT1 ablation and acetylation deficiency of GNPAT repress lipid metabolism and tumor progression in xenograft and DEN/CCl_4-induced HCC. Otherwise, ACAT1 inhibitor combination with sorafenib enormously retards tumor formation in mice. Collectively, we demonstrate that stabilization of FASN by ACAT1-mediated GNPAT acetylation plays a critical role in hepatocarcinogenesis.

Introduction

Fatty acid synthase (FASN) is a critical enzyme for the synthesis of long-chain fatty acids from malonyl-CoA [1] and FASN upregulation has been identified in many cancer types, such as prostate cancer [2], pancreatic cancer [3], breast cancer [4], and colorectal cancer [5]. FASN is highly related with cancer biological aggressiveness and unfavorable prognosis [6]. FASN overexpression in tumor is dependent on the PI3K–AKT signal transduction pathway and SREBP 1c transcriptional regulation [7, 8]. Moreover, USP2a regulated the stability of FASN in prostate cancer [9], while TIRM21-mediated FASN ubiquitination promoted its degradation [10]. Thus, targeting FASN for cancer therapy provides an attractive approach [1].

Glyceronephosphate O-acyltransferase (GNPAT) is a critical rate-limiting enzyme in the biosynthesis of plasmalogens (PIs) and also contributes to the synthesis of fatty acid (FA) [11]. GNPAT knockout mice have been indicated to exhibit substantial defects in eye development, male infertility [12], blood–testis barrier [13], motor defects, and muscle strength with altered neuromuscular junction [14]. Inflammation stimuli reduced GNPAT expression through enhanced c-Myc recruitment onto the GNPAT promoter [15]. GNPAT is also significant for the maturation of semiinvariant natural killer T cells [16]. Recently, we found that GNPAT was amplified and upregulated in HCC patients, and recruited USP30 to stabilize DRP1, leading to promotion of lipid uptake, synthesis, and HCC progression [17]. However, how GNPAT promotes lipogenesis and cancer development remains unclear.

Acetyl-CoA Acetyltransferase 1 (ACAT1), a mitochondrial enzyme, converts two acetyl-CoA molecules to acetoacetyl-CoA and CoA in ketogenesis [18]. It has been reported that ACAT1 and SIRT3 acted as the upstream acetyltransferase and deacetylase, respectively, of PDHA1 and PDP1 [19]. Moreover, tetrameric ACAT1 was more active and phosphorylated in Y407 through the

Supplementary information The online version of this article (https://doi.org/10.1038/s41388-020-1156-0) contains supplementary material, which is available to authorized users.

✉ Li Gu
gulicherry@whu.edu.cn

✉ Youjun Li
liy7@whu.edu.cn

[1] Hubei Key Laboratory of Cell Homeostasis, College of Life Sciences, Wuhan University, Wuhan 430072, China

[2] Medical Research Institute, School of Medicine, Wuhan University, Wuhan 430071, China

Published online: 23 January 2020

PDHA1-PDK1 axis to promote glycolysis and cancer cell proliferation [20].

In this report, we identified that GNPAT was acetylated by ACAT1 at K128 under PA stimulation and dissociated SIRT4-mediated deacetylation. GNPAT acetylation repressed TRIM21-mediated GNPAT and FASN ubiquitination and degradation. GNPAT acetylation favored tumor growth in xenograft and DEN/CCl_4-induced mouse HCC. Moreover, ACAT1 depletion repressed tumor progression and combination of ACAT1 inhibitor with sorafenib retarded HCC development to a great extent in mice, which indicates a potential novel anticancer strategy in HCC.

Results

ACAT1 acetylates GNPAT at K128

As we have found that GNPAT was upregulated and promoted FAs synthesis in HCC [17], we were exciting to explore whether FA affects GNPAT in a feedback loop. SDS-PAGE and Mass Spectrometry (MS) were conducted following ectopic GNPAT expression in the presence and absence of PA induction. Fortunately, the acetyltransferase ACAT1 was identified to abundantly be pulled down by GNPAT, especially with PA induction (Fig. 1a). Reciprocally,

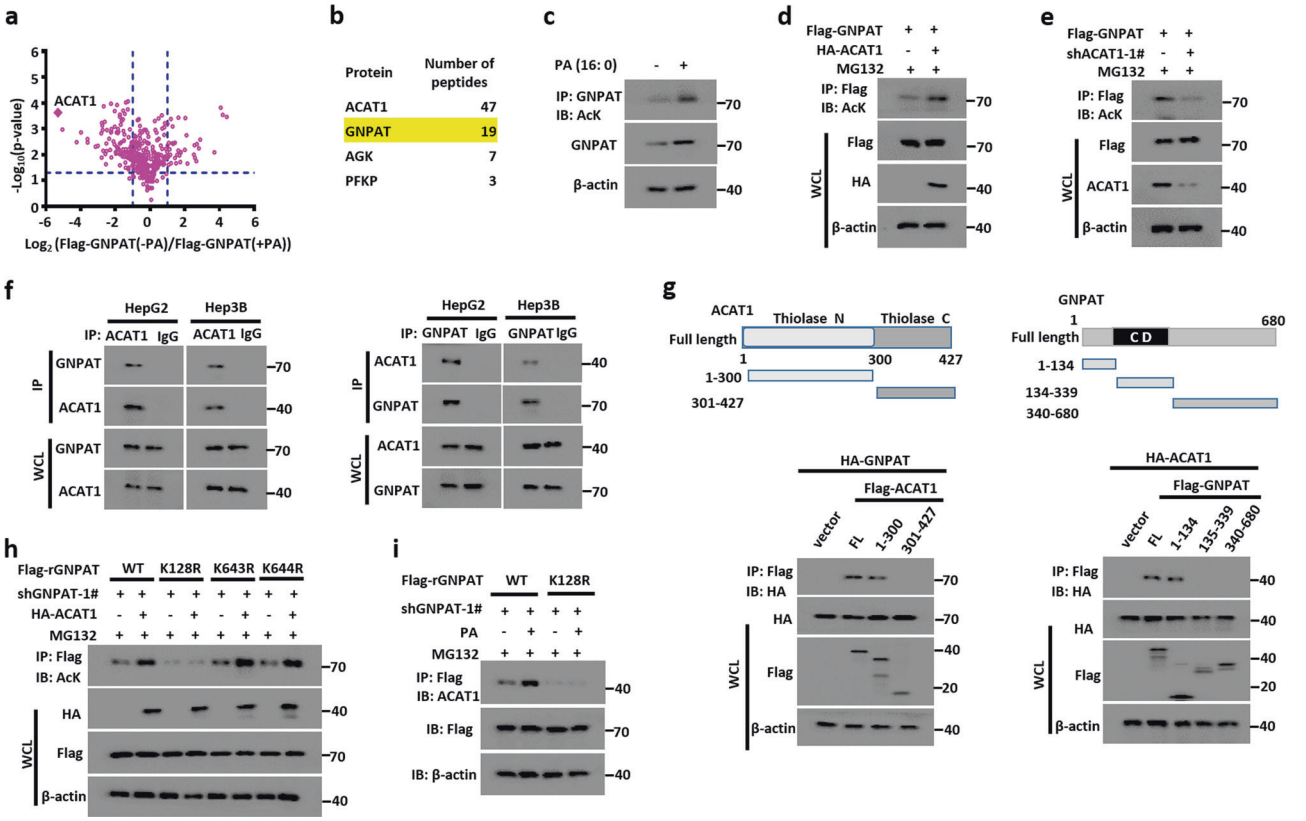

Fig. 1 ACAT1 acetylates GNPAT. a Cellular extracts from HEK293 cells expressing Flag-GNPAT in the absence and presence of palmitic acid (PA) (0.4 mM) for 12 h were immunopurified with anti-Flag affinity columns. The eluates were resolved by SDS-PAGE and Coomassie blue staining. The whole bands were retrieved and analyzed by mass spectrometry (MS). Scatterplots displayed comparisons of GNPAT overexpressing cells in the absence and presence of PA. **b** GNPAT was pulled down in MS data with HEK293 empty cells compared with Flag-ACAT1 overexpression. **c** Pan-acetyl-lysine (α-AcK) level of GNPAT was upregulated in cells treated with PA (0.4 mM). Flag-tagged GNPAT and HA-ACAT1 (**d**) or shACAT1 (**e**) were co-expressed in HEK293. IP with Flag antibody and IB with AcK antibodies. **f** Endogenous interaction between ACAT1 and GNPAT. Whole cell lysates from HepG2 (left) and Hep3B (right) cells were prepared and IPs were performed with antibodies against the indicated proteins. Immunocomplexes were then immunoblotted using antibodies against GNPAT and ACAT1. **g** Schematic diagram showed the structure of ACAT1 (left) and GNPAT (right) and truncation mutants were used. Flag-tagged ACAT1 wild-type or truncation mutants were co-expressed with HA-GNPAT in HEK293. Extracts were immunoprecipitated with Flag antibody and examined by western blotting (left). Flag-tagged GNPAT wild-type or truncation mutants were co-expressed with HA-ACAT1 in HEK293. Co-IP with Flag antibody and examined by indicated antibodies (right). **h** ACAT1 acetylated GNPAT at K128. **i** GNPAT K128R mutant decreased the interaction between GNPAT and ACAT1. HEK293 cells were co-transfected with indicated constructs with or without PA induction. IP with Flag and IB with ACAT1 antibody.

GNPAT was efficiently co-immunoprecipitated with ACAT1 (Fig. 1b). And the acetylation of GNPAT was found to be largely elevated with PA induction by a pan-acetyl lysine antibody (α-Ack) (Fig. 1c). Simultaneously, stearic acid (SA) also induced GNPAT acetylation (Supplementary Fig. 1a), indicating that saturated FAs favored GNPAT acetylation. Immunoprecipitation (IP) of GNPAT tested that ACAT1 indeed facilitated GNPAT acetylation (Fig. 1d). Conversely, knockdown of ACAT1 inhibited GNPAT acetylation (Fig. 1e), while this defect was rescued with ectopic ACAT1 expression (Supplementary Fig. 1b). PA stimulation also increased ACAT1 protein expression without its mRNA level alteration (Supplementary Fig. 1c). Then we checked whether PA affected ubiquitination of ACAT1. As supposed, ACAT1 ubiquitination was largely decreased in regardless of endogenous or exogenous ACAT1 (Supplementary Fig. 1d, e). However, ACAT2 could not alert GNPAT acetylation (Supplementary Fig. 1f, g).

Next, we testified whether ACAT1 interacted with GNPAT. The acetyltransferases from MS were checked, and only ACAT1 interacted with GNPAT, rather than ACAT2, HAT1, or KAT7 (Supplementary Fig. 1h). The interaction between GNPAT and ACAT1 was also confirmed by the endogenous Co-IP experiment in HCC HepG2 and Hep3B cells (Fig. 1f). Moreover, the thiolase N domain of ACAT1 and N-terminal of GNPAT were necessary to interact with each other (Fig. 1g). Then the acetylation sites were predicted through the website (https://www.phosphosite.org). We mutated each predicted site with lysine (K) to arginine (R), and identified that only K128R, rather than K643R or K644R, greatly abrogated the increased acetylation of GNPAT (Fig. 1h), which was also within GNPAT N-terminal domain that interacted with ACAT1. Lysine 128 of GNPAT was also conserved from homo sapiens to monkey (Supplementary Fig. 1i). And $GNPAT^{K128R}$ enormously disrupted the interaction between GNPAT and ACAT1 with PA induction (Fig. 1i). All together, we identified a novel GNPAT acetyltransferase ACAT1 that acetylated GNPAT at K128.

GNPAT is deacetylated by SIRT4 at K128

As acetylation is a reversible modulation, we investigated the deacetyltransferase of GNPAT. We found that only treated with nicotinamide (NAM), an inhibitor of the SIRT family deacetylases, could enhanced the GNPAT acetylation, while trichostatin A (TSA), inhibitor of histone deacetylase class, had no effect (Fig. 2a). As GNPAT is mainly localized in peroxisome and mitochondria, we searched for the SIRT deacetylases that reside in mitochondria, namely SIRT1-5. Co-IP experiments indicated that SIRT4 and SIRT5 could be both pulled down by GNPAT, while only ectopic SIRT4 expression reduced GNPAT acetylation (Fig. 2b, c). And this could be reversed by catalytically inactive SIRT4 mutant (H161Y) (Fig. 2d). Conversely, shRNA-mediated SIRT4 depletion augmented GNPAT acetylation (Fig. 2e). SIRT4 inhibition also enhanced GNPAT protein level without mRNA level alteration (Supplementary Fig. 2a), and this defect was rescued by SIRT4 wild type (WT) but not SIRT4 (H161Y) (Supplementary Fig. 2b). Furthermore, ectopic expression of WT, but not H161Y mutant, led to a decrease in GNPAT protein level (Fig. 2f). Cycloheximide (CHX) chase experiment also confirmed SIRT4 suppression largely enhanced the half-life of GNPAT (Supplementary Fig. 2c).

Similarly, endogenous interaction between SIRT4 and GNPAT was identified in HCC cells (Fig. 2g) and SIRT4 deacetylated GNPAT at K128 (Fig. 2h). Moreover, we investigated that whether SIRT4 could antagonize ACAT1-mediated GNPAT acetylation. The results indicated that ectopic SIRT4 expression could decrease the enhanced GNPAT acetylation in HepG2 and Hep3B, while SIRT4 depletion slightly rescued the reduction of GNPAT acetylation caused by ACAT1 inhibition (Fig. 2i, j and Supplementary Fig. 2d, e). Above all, we discovered that SIRT4 deacetylated GNPAT at K128 with dissociation of ACAT1.

ACAT1 stabilizes GNPAT by acetylation at K128

As ACAT1 facilitated GNPAT acetylation, we next investigated whether ACAT1 promoted GNPAT stabilization. ACAT1 depletion largely reduced GNPAT protein level, while the mRNA level was not changed (Fig. 3a). ACAT1 depletion was associated with shortened half-life of GNPAT (Fig. 3b). Then we generated $GNPAT^{K128Q}$ mutant with glutamine (Q) instead of lysine (K), and found that $GNPAT^{K128Q}$ was more stable than $GNPAT^{K128R}$ (Fig. 3c). PA induction prolonged the GNPAT half-life as well (Fig. 3d). Moreover, MG132, rather than NH_4Cl or 3-MA, inhibited the reduction of GNPAT protein level with ACAT1 depletion (Fig. 3e), suggesting that ACAT1 inhibition mediated GNPAT degradation through the proteasome pathway.

In addition, we did amino acid sequence analysis of dimerization motif [G/S/A/L/I]-XXX-[G/S/A/L/I] [21] in GNPAT N-terminal domain and found nine motifs were suitable for GNPAT dimerization (Fig. 3f). Cross-linking results indicated that ACAT1 knockdown largely converted GNPAT from dimers to monomers (Fig. 3g). In addition, Co-IP demonstrated that ACAT1 promoted GNPAT dimerization, and acetylation deficient $GNPAT^{K128R}$ mutant reduced GNPAT oligomerization and $GNPAT^{K128Q}$ mildly increased GNPAT oligomerization (Fig. 3h, i). Together, we found that ACAT1 promoted GNPAT stabilization and dimerization.

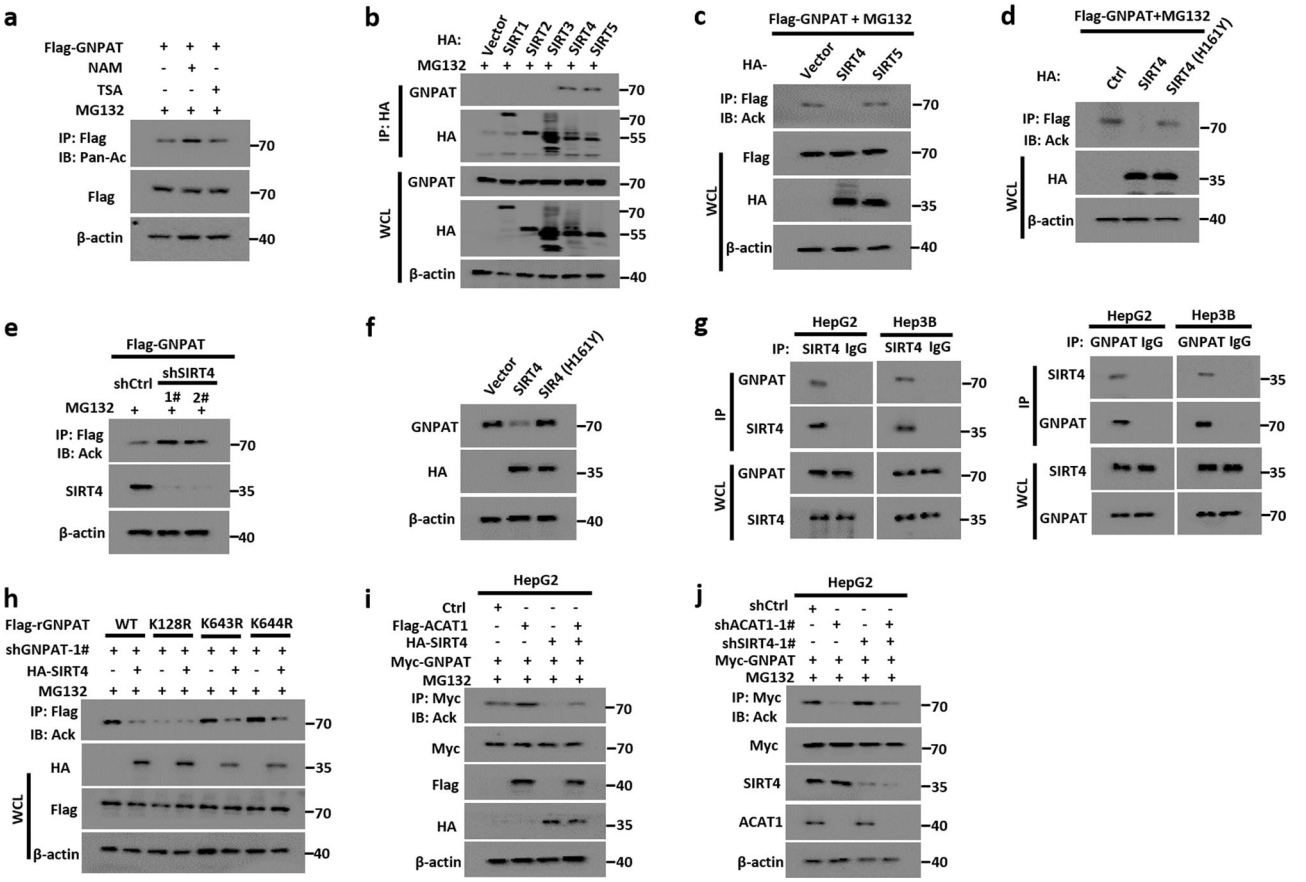

Fig. 2 SIRT4 deacetylates GNPAT at K128. a Exogenous GNPAT is deacetylated. HEK293T cells were treated with NAM (20 mM) or TSA (10 μM) for 6 h and then IP and IB were performed with the indicated antibodies. **b** GNPAT interacted with SIRT4 and SIRT5. Ectopic expression of HA-tagged SIRT1-5 then IP with HA beads and IB with indicated antibodies. **c** Acetylation levels were tested with co-expressing SRIT4 or SIRT5 and GNPAT. Flag-GNPAT was co-expressed with WT-SIRT4 or SIRT4 (H161Y) (**d**) or SIRT4 shRNAs (**e**). IP with Flag and IB with indicated antibodies. **f** GNPAT protein level was identified with SIRT4 WT or SIRT4 (H161Y) expression. **g** Endogenous interaction between SIRT4 and GNPAT. IP and IB with indicated antibodies. **h** SIRT4 deacetylated GNPAT at K128. HEK293 cells were transfected with indicated vectors, IP and IB analysis were performed with the indicated antibodies. **i**, **j** SIRT4 antagonized ACAT1-mediated acetylation of GNPAT. HepG2 cells were transfected with indicated vectors, IP and IB analysis were performed with the indicated antibodies.

Acetylation inhibits GNPAT degradation via the ubiquitin–proteasome pathway

As ACAT1 stabilized GNPAT and hindered proteasome degradation, we next investigated whether ACAT1 repressed GNPAT degradation through the ubiquitin–proteasome pathway. ACAT1 depletion accelerated GNPAT ubiquitination while ectopic ACAT1 expression had the opposite effect (Fig. 4a and Supplementary Fig. 3a). GNPAT acetylation mutant K128R facilitated GNPAT ubiquitination, while GNPAT ^{K128Q} largely abrogated GNPAT ubiquitination (Fig. 4b).

Then we investigated the ubiquitinase that promoted GNPAT ubiquitination. TRIM21, CUL3, and CUL5 were identified from IP/MS, and IP tested that only TRIM21 interacted with GNPAT (Fig. 4c). Endogenous interaction were confirmed in HepG2 and Hep3B, and the RING domain of TRIM21 interacted with GNPAT (Supplementary Fig. 3b, c). Ectopic ACAT1 expression impaired the interaction between GNPAT and TRIM21, while acetylation deficient of GNPAT (K128R) enhanced the interaction (Fig. 4d and Supplementary Fig. 3d), indicating that the acetylation repressed their interaction.

Co-IP experiment indicated that TRIM21 facilitated GNPAT ubiquitination while RING domain deletion (ΔRING) eliminated this effect (Fig. 4e). And TRIM21 depletion suppressed GNPAT ubiquitination (Supplementary Fig. 3e). We then mutated the predicted ubiquitination sites with K113R, K146R, and K312R, and identified that all of the three mutants decreased GNPAT ubiquitination (Fig. 4f), and GNPAT K113R/146R/312R (3KR) abundantly abrogated GNPAT ubiquitination (Supplementary

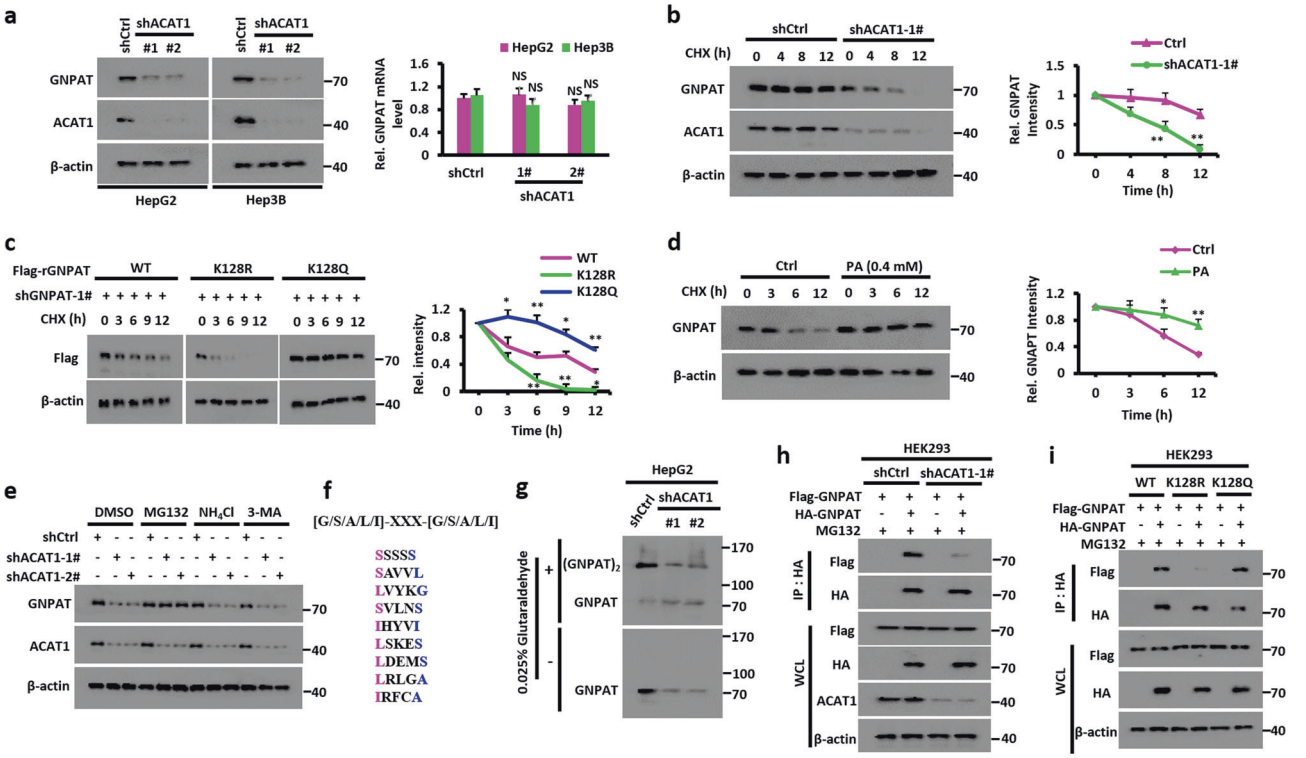

Fig. 3 ACAT1 stabilizes GNPAT by its acetylation at K128. a Western blot (left) and RT-qPCR assay (right) of GNPAT level upon ACAT1 knockdown in HCC cells HepG2 and Hep3B. **b**, **c** Acetylation affects GNPAT protein turnover. HepG2 (**b**) or HEK293 (**c**) cells were transfected with indicated vectors. After cells were treated with CHX (50 μg/ml) for the indicated time, expression of GNPAT and ACAT1 were analyzed by western blotting (left); the intensity of GNPAT expression for each time point was quantified by densitometry with β-actin as a normalizer (right). **d** PA induction affects protein turnover. HEK293 cells were collected after PA (0.4 mM) treatment for 12 h. The intensity of GNPAT expression for each time point was quantified by densitometry with β-actin as a normalizer (right). **e** Immunoblotting analysis of GNPAT protein expression in HEK293 cells transfected with shACAT1 after treatment with NH_4Cl (25 mM), MG132 (100 μM), or 3-MA (500 ng/ml) for 6 h. **f** The dimerization motifs of GNPAT were identified in GNPAT N-terminal. **g** ACAT1 knockdown reduced endogenous GNPAT dimerization. Endogenous GNPAT was immunopurified from HepG2 cells stably expressing shCtrl and ACAT1 shRNAs. **h**, **i** ACAT1 promotes GNPAT dimerization. HEK293 were transfected with indicated vectors. IP and IB with indicated antibodies. Data were presented as mean ± SD. $*P < 0.05$, $**P < 0.01$, $***P < 0.001$.

Fig. 3f). Moreover, ectopic TRIM21 expression promoted $GNPAT^{K128R}$ ubiquitination but had no effect on $GNPAT^{K128Q}$ mutants (Supplementary Fig. 3g). Next we identified the type of TRIM21 modulated GNPAT ubiquitination with different ubiquitin mutants. We found that retain of the site K27, K33, and K48 (K-O) increased GNPAT ubiquitination (Fig. 4g), suggesting that TRIM21 ubiquitinated GNPAT in K113, K146, and K312 through K27, K33, and K48-linked ubiquitination.

In addition, we investigated whether TRIM21-mediated GNPAT ubiquitination impacted GNPAT stabilization. The luciferase assay with the GNPAT ORF fused to the reconstructive reporter [22] (GNPAT-Luc) indicated that TRIM21 largely reduced GNPAT protein level (Fig. 4h). TRIM21 depletion increased GNPAT protein level without affected its mRNA level (Fig. 4i). $GNPAT^{3KR}$, mutation of ubiquitination sites, largely stabilized GNPAT (Supplementary Fig. 3h). Collectively, we discovered that TRIM21-mediated GNPAT ubiquitination and degradation through K27, K33, and K48-ubiquitin at K113, K146, and K312.

GNPAT represses TRIM21-mediated FASN degradation and promotes lipogenesis

To further identify how GNPAT enhanced lipid synthesis, we discovered FASN, a terminal enzyme in the de novo lipogenesis, was abundantly existed in the MS data. Endogenous co-IP indicated that FASN was closely interacted with GNPAT in HepG2 and Hep3B cells (Fig. 5a). Moreover, we identified that GNPAT acetylation promoted their interaction (Fig. 5b and Supplementary Fig. 4a). With acetylation site mutant, we testified that GNPAT (K128R) largely disrupted the interaction of GNPAT and FASN, while GNPAT (K128Q) facilitated this effect. Then we checked if GNPAT affected FASN stabilization. Actually, depletion of GNPAT inhibited FASN protein level and abrogated FASN activity (Fig. 5c and Supplementary Fig. 4b). The CHX assay also demonstrated that GNPAT inhibition attenuated FASN half-life, while ectopic GNPAT expression largely promoted FASN stability (Fig. 5d and Supplementary Fig. 4c–e). GNPAT acetylation mutant

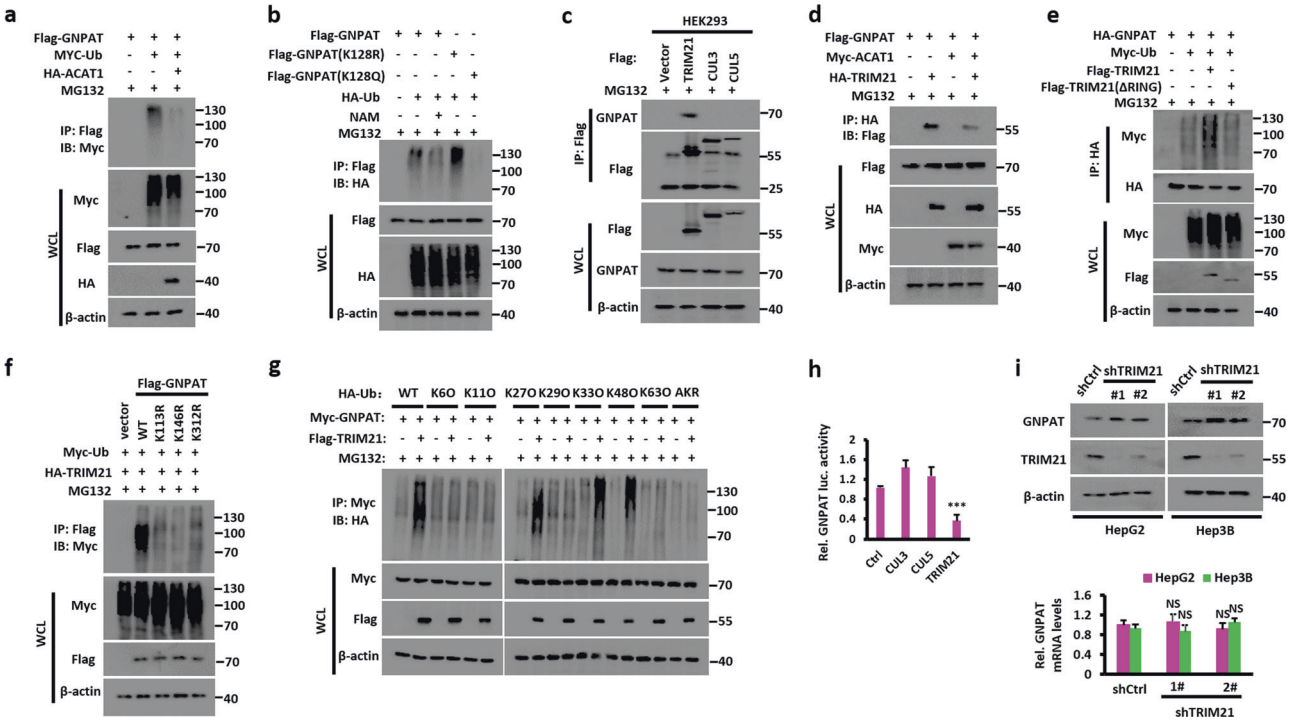

Fig. 4 GNPAT acetylation impairs TIRM21-mediated ubiquitination and degradation. a, **b** ACAT1 repressed GNPAT ubiquitination. HEK293 cells were co-expressed with different vectors and treated with MG132 (100 μM) or NAM (20 mM). IP and IB with indicated antibodies. **c** Exogenous TRIM21, CUL3, or CUL5 were expressed and IP with Flag and IB with indicated antibodies. **d** ACAT1 inhibited the interaction between GNPAT and TRIM21. **e** The RING domain was required for TRIM21-mediated ubiquitination of GNPAT. **f** TRIM21 ubiquitinates GNPAT at K113/146/312. **g** TRIM21-mediated K27/33/48-linked ubiquitination of GNPAT. **d**–**g** HEK293 cells were co-expressed with different vectors. IP and IB with indicated antibodies. **h** The luciferase assay for expressing the indicated vectors in HEK293. **i** Western blot (upper) and qRT-PCR assay (bottom) of GNPAT levels with TRIM21 knockdown. Data were presented as mean ± SD. ***$P < 0.001$.

(K128R) promoted FASN ubiquitination but GNPAT acetylation mimic mutation (K128Q) repressed the ubiquitination (Fig. 5e). Moreover, we identified that GNPAT suppressed FASN ubiquitination rather than GNPAT-ΔCD (Supplementary Fig. 4f).

As Lin. et al. have found that TRIM21 ubiquitinated FASN and promoted FASN degradation [10], next we evaluated whether GNPAT repressed TRIM21-induced FASN degradation. Ectopic GNPAT expression largely inhibited TRIM21 induced FASN ubiquitination (Fig. 5f). Moreover, TRIM21 depletion attenuated the ubiquitination of FASN with GNPAT abrogation (Supplementary Fig. 4g). Further, ectopic GNPAT expression promoted FASN expression and activity which was reduced by ectopic TRIM21 expression. Suppression of GNPAT lessened FASN expression and activity which was rescued by TRIM21 inhibition (Supplementary Fig. 4h, i). Altogether, we identified that GNPAT promoted FASN stability with repression of TRIM21-mediated FASN ubiquitination.

Then we evaluated whether FASN-GNPAT affected lipid metabolism. FASN overexpression largely promoted TG, FAs level, and lipid synthesis from acetate in HepG2 and Hep3B cells, while with GNPAT inhibition slightly decreased the TG, FAs, and lipogenesis (Fig. 5g–i and Supplementary Fig. 4j). Conversely, GNPAT overexpression as well as FASN depletion could not rescue the lipid metabolism level (Fig. 5j–l and Supplementary Fig. 4k). Above all, we discovered that GNPAT promoted tumor metabolism through FASN.

GNPAT acetylation promotes xenograft tumor growth

To investigate the effect of GNPAT acetylation on tumor growth, we constructed GNPAT knockout cells with CRISPER/Cas9 technology. Then stable cell lines which stably expressed GNPAT WT, K128R, and K128Q mutants were established in HepG2 and Hep3B GNPAT knockout cells. A total of 5×10^6 of the individual cells were subcutaneous injected to the nude mice and sacrificed after 35 days. $GNPAT^{K128R}$ retarded tumor growth while $GNPAT^{K128Q}$ accelerated xenograft growth (Fig. 6a–c). As GNPAT promoted FAs synthesis, we tested whether GNPAT acetylation influenced lipid metabolism. Acetylation deficient $GNPAT^{K128R}$ decreased triglyceride (TG) and FAs level and lipogenesis with ^3H labeled acetate to trace

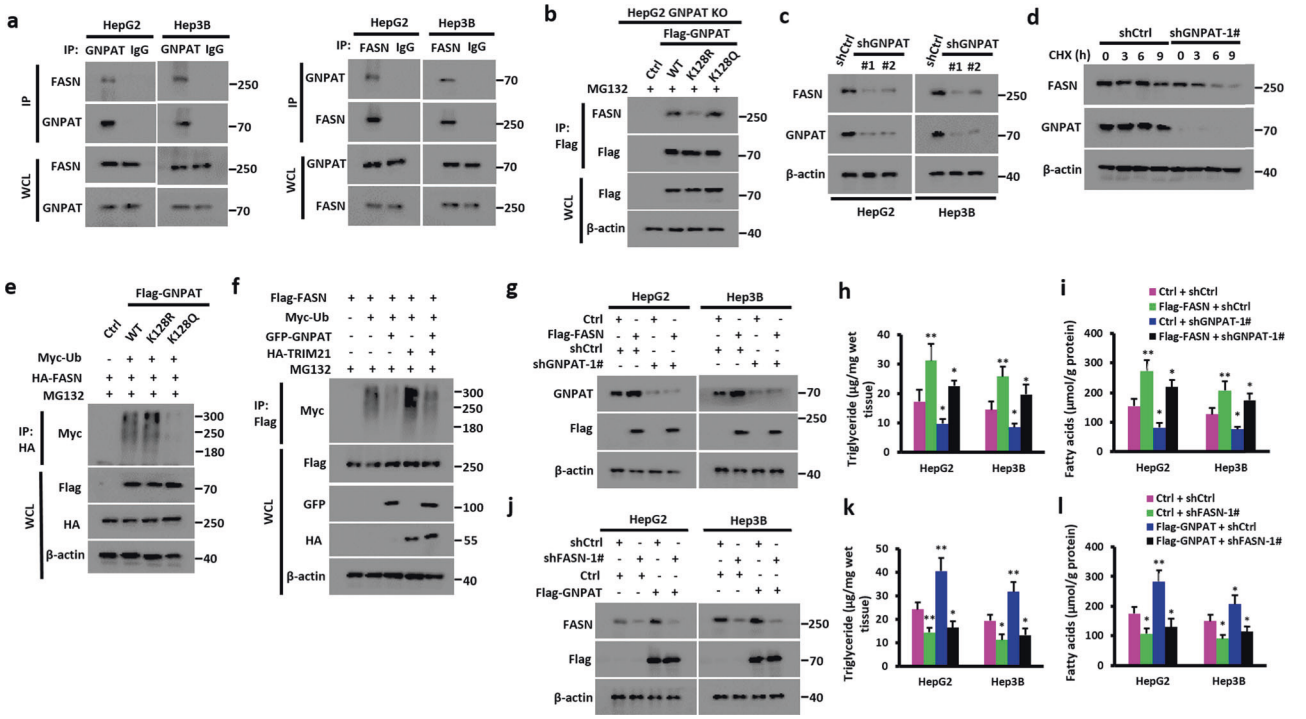

Fig. 5 GNPAT represses TRIM21-mediated FASN degradation and promotes lipogenesis. a Endogenous interaction between FASN and GNPAT. Whole cell lysates from HepG2 (left) and Hep3B (right) cells were prepared and IPs were performed with antibodies against the indicated proteins. Immunocomplexes were then immunoblotted using antibodies against GNPAT and FASN. **b** GNPAT acetylation mutant K128R inhibited the interaction between GNPAT and FASN, and GNPAT K128Q promoted the mutual interaction in HepG2 cells. Cells were transfected with indicated vectors. IP with Flag and IB with indicated antibodies. **c** The western blot assay of FASN levels in GNPAT-depleted cells in HepG2 and Hep3B. **d** GNPAT inhibition affects FASN protein turnover. HEK293 cells were transfected with indicated vectors. After cells were treated with CHX (50 μg/ml) for the indicated time, expression of FASN and GNPAT were analyzed by western blotting. **e** GNPAT acetylation mutant K128R increased the FASN ubiquitination and GNPAT K128Q decreased the ubiquitination of FASN. **f** GNPAT inhibited FASN ubiquitination, and this can be rescued by TRIM21 overexpression. **g**, **j** The western blot assay of indicated proteins in HepG2 and Hep3B. **h**, **k** The trigyceride levels of indicated cells from **g**, **j**. **i, l**. The fatty acids levels of indicated cells from **g**, **j**. Data are presented as mean ± SD. $^{*}P < 0.05$, $^{**}P < 0.01$.

lipid synthesis, while acetylation mimic GNPAT^{K128Q} enhanced the lipid metabolism as shown increasing FA synthesis and TG level (Fig. 6d–f).

Arecoline hydrobromide (AH) was reported to effectively inhibit ACAT1 activation [20] and sorafenib was the most effective drug approved for the treatment of advanced HCC [23]. To enhance the anticancer activity and reduce the drug resistance, we considered that combination of AH with Sorafenib for HCC therapy. Xenograft experiments with intraperitoneal injection of AH and sorafenib, respectively, slightly reduced tumor growth and combination therapy abnormally decreased tumor volume and weight (Fig. 6g–i). Moreover, combination AH with sorafenib reduced lipid metabolism in vivo (Fig. 6j–l).

GNPAT mediates ACAT1 oncogenic phenotypes

Next, we assessed whether oncogenic phenotype of ACAT1 was dependent on GNPAT. We found that ectopic ACAT1 expression promoted tumor growth in xenograft mice and meanwhile GNPAT depeletion attenuated tumor growth (Supplementary Fig. 5a–c), and ectopic ACAT1 expression with GNPAT inhibition slightly diminished FAs synthesis, TG, and lipogenesis level (Supplementary Fig. 5d–f).

Conversely, ACAT1 abrogation impeded tumor growth and ectopic GNPAT expression largely rescued the phenotype in vivo (Supplementary Fig. 5g–i). Similarly, ACAT1 repression with GNPAT overexpression confirmed the results in lipid metabolism (Supplementary Fig. 5j–l). Above all, we found that GNPAT modulated ACAT1 oncogenic phenotypes.

GNPAT acetylation enhances DEN/CCl_4-induced hepatocarcinogenesis in mice

We then examined the expression of ACAT1, SIRT4, TRIM21, and FASN in an autologous HCC model induced by a combination of diethylnitrosamine (DEN) and carbon tetrachloride (CCl_4). ACAT1, GNPAT, and FASN were gradually upregulated and SIRT4 and TIRM21 were downregulated at various times during disease development (Supplementary Fig. 6a).

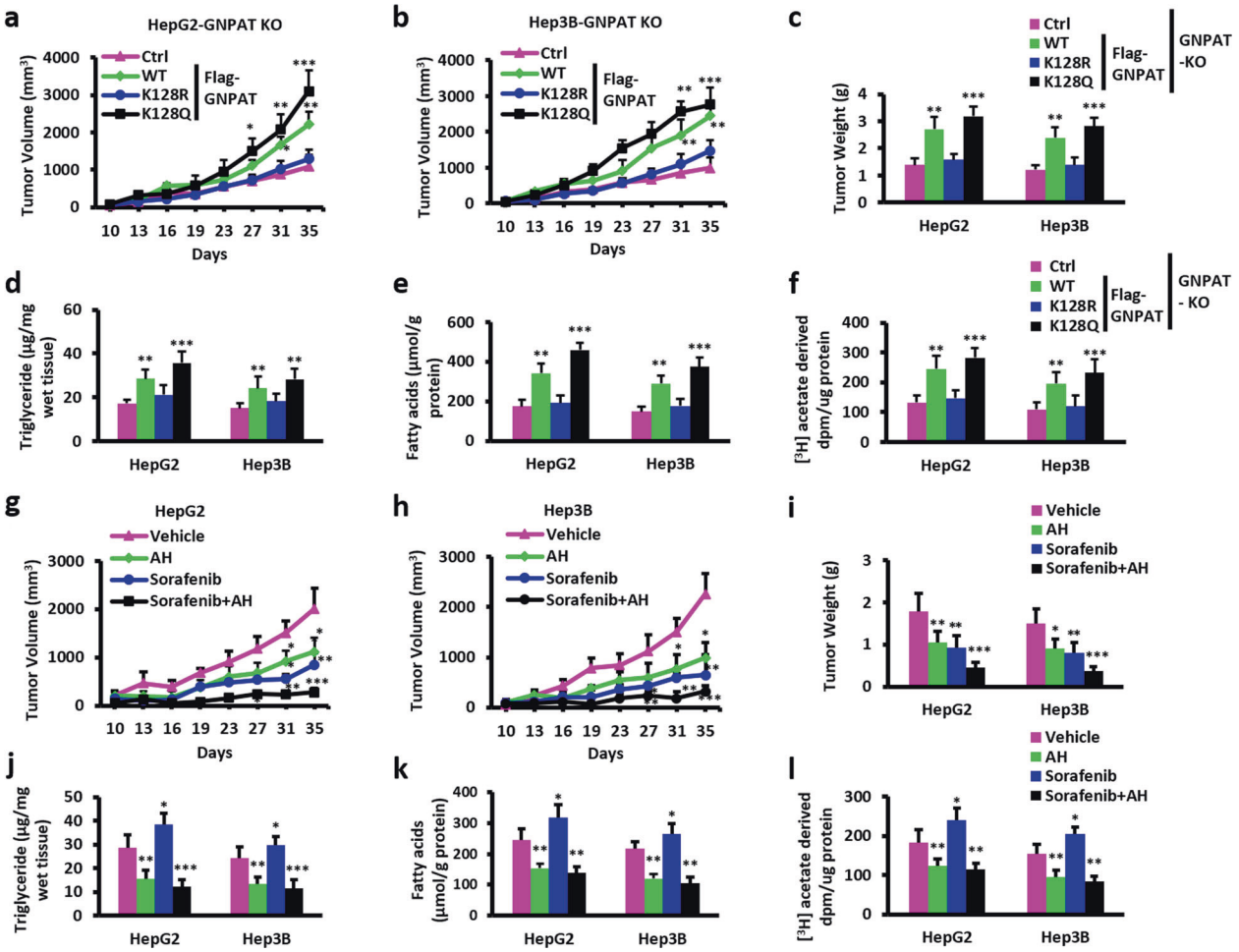

Fig. 6 ACAT1-mediated GNPAT acetylation promotes tumor growth. a, **b** Xenograft growth in nude mice stably expressing GNPAT WT, K128R, or K128Q mutants with indicated antibodies in HepG2 and Hep3B cells. Cells with stably expressing GNPAT constructs were injected subcutaneously into nude mice ($n = 5$). Tumor volumes were measured every 3–4 days. Tumor growth curve after injecting the indicated cells. Tumor weight (**c**), liver TG levels (**d**), NEFA (**e**), and incorporation of [^{3}H] acetate into neutral lipids levels (**f**) in xenograft tumors. **g–i** Intraperitoneal injection with AH (50 mg/kg, once every other day) or sorafenib (30 mg/kg, once every other day) or combination AH (50 mg/kg) and sorafenib (30 mg/kg) once every other day to the xenograft mice 10 days later after injected with indicated cells. Tumor volume (**g**, **h**) and weight (**i**) were calculated for each group. TG (**j**), fatty acids (**k**), and lipid synthesis levels (**l**) from indicated tumors. Data were presented as mean ± SD. $^*P < 0.05$, $^{**}P < 0.01$, $^{***}P < 0.001$.

To investigate whether ACAT1 inhibition attenuated autologous HCC tumor growth in the above model, concentrated adeno-associated virus (AAV) containing AAV8-shAcat1 expression vector were administered to DEN/CCl_4-treated mice and the tumor burden was assessed at week 30 (Fig. 7a). Tumors treated with AAV8-shAcat1 were smaller and showed reduced expression of ACAT1, GNPAT, and Ack-GNPAT (Fig. 7b, c). ACAT1 repression showed less tumor nodules, tumor weight, and tumor volume (Fig. 7d, e and Supplementary Fig. 6b). Moreover, The mRNA level of related lipogenesis and FA uptake genes were down-regulated mostly (Supplementary Fig. 6d, e), and ACAT1 knockdown reduced TG and FA levels as well (Fig. 7f, g and Supplementary Fig. 6c).

Next, we explored the effects of the GNPAT acetylation mutants in DEN/CCl_4-induced HCC. Just as the xenograft, $GNPAT^{K128R}$ retarded liver tumor growth, while $GNPAT^{K128Q}$ accelerated HCC progression (Fig. 7h–k). And acetylation mutants of GNPAT showed similar tendency in lipid metabolism (Fig. 7l–n).

Suppression of DEN/CCl_4-induced hepatocarcinogenesis by combination of ACAT1 inhibitor and sorafenib in mice

With DEN/CCl_4-induced HCC, we treated with ACAT1 inhibitor (AH), sorafenib, respectively and combination. Treatment with AH or sorafenib moderately attenuated liver tumor growth, while combination of AH and sorafenib severely reduced tumor sizes and numbers (Fig. 8a, b and Supplementary Fig. 7a, b). Combination therapy with AH and sorafenib also greatly decreased TG and FA levels, and

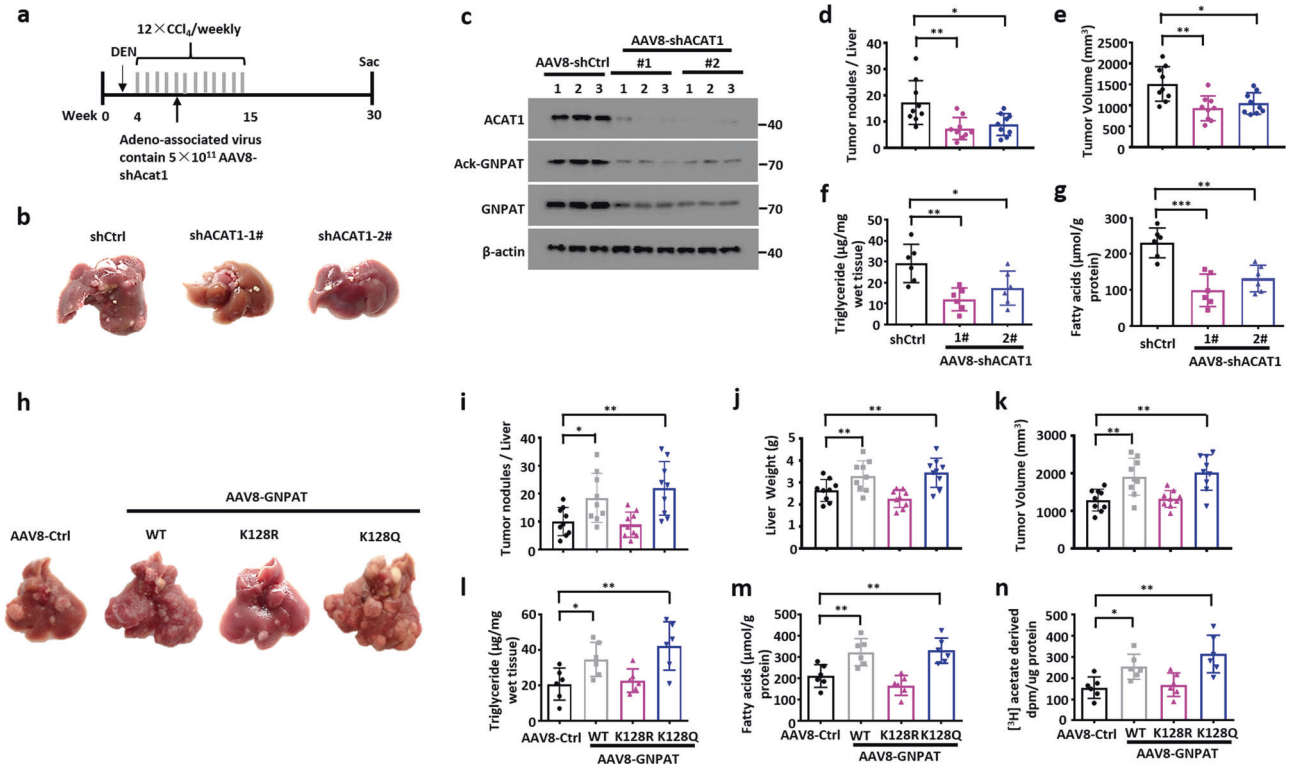

Fig. 7 ACAT1 inhibition and GNPAT acetylation attenuates and enhances DEN/CCl_4-induced hepatocarcinogenesis in mice, respectively. a The schematic overview of DEN/CCl_4-induced HCC mice model. DEN (25 mg/ml) was injected 15 days after birth ($n = 10$). From 4–15 weeks, mice were intraperitoneal injected with CCl_4 (0.5 ml/kg) weekly. During this period, adeno-associated virus containing Acat1 shRNAs were given via tail-vein injection. After 30 weeks, livers were extracted. **b** Liver images extracted from the indicated mice. **c** Western blot analysis of the indicated protein expression of liver tissues from (**a**). Tumor nodules (**d**) and tumor volume (**e**) of each liver. Liver TG (**f**) and fatty acids (**g**) levels in mice from (**a**). **h** Adeno-associated virus containing AAV8-GNPAT WT or mutants were injected to the mice through tail-vein. Liver images extracted from the indicated mice. Tumor nodules (**i**), Liver weight (**j**), and tumor volume (**k**) of each liver. Liver TG (**l**), fatty acids (**m**), and lipogenesis (**n**) levels in mice from **h**. Data were presented as mean ± SD. $^*P < 0.05$, $^{**}P < 0.01$, $^{***}P < 0.001$.

reduced the lipid synthesis (Fig. 8c, d and Supplementary Fig. 7c), suggesting that combination Sorafenib with AH might be superior to the sorafenib alone in HCC therapy.

GNPAT acetylation and ACAT1 are upregulated in HCCs

To identify ACAT1-mediated GNPAT acetylation might be better targets in HCC patients, we assessed their expression in 24 pairs of clinical HCC patients with adjacent nontumor tissues by western blot. Firstly, we found that ACAT1 mRNA level was the highest in HCC among different cancers in the Human Protein Atlas (Supplementary Fig. 7d). The results showed that GNPAT acetylation, ACAT1 and FASN were highly expressed in most of the patients, and SIRT4 and TRIM21 were downregulated (Fig. 8e–i and Supplementary Fig. 7e). ACAT1 had a greatly positive correlation with GNPAT and its acetylation while SIRT4 and TRIM21 was negatively correlated with GNPAT and its acetylation (Fig. 8j–n). Altogether, we discovered that GNPAT acetylation, ACAT1 and FASN were upregulated in HCC patients.

Discussion

HCC is the second most frequent cause of cancer-related death world-wide [24], and metabolic reprogramming has been demonstrated more and more significantly in carcinogenesis [25]. In our current work, we discovered a new mechanism that FAs stabilized GNPAT through ACAT1 acetylation, whereas SIRT4 deacetylated GNPAT. GNPAT acetylation restrained TRIM21-mediated ubiquitination and degradation of GNPAT. Moreover, GNPAT stabilized FASN and repressed TRIM21-mediated FASN degradation and promoted lipid metabolism and hepatocarcinogenesis (Fig. 8o). Combination of ACAT1 inhibitor AH with sorafenib effectively retarded tumor development in xenograft and DEN/CCl_4-induced HCC, suggesting that ACAT1 inhibition might be a potential target in HCC therapy.

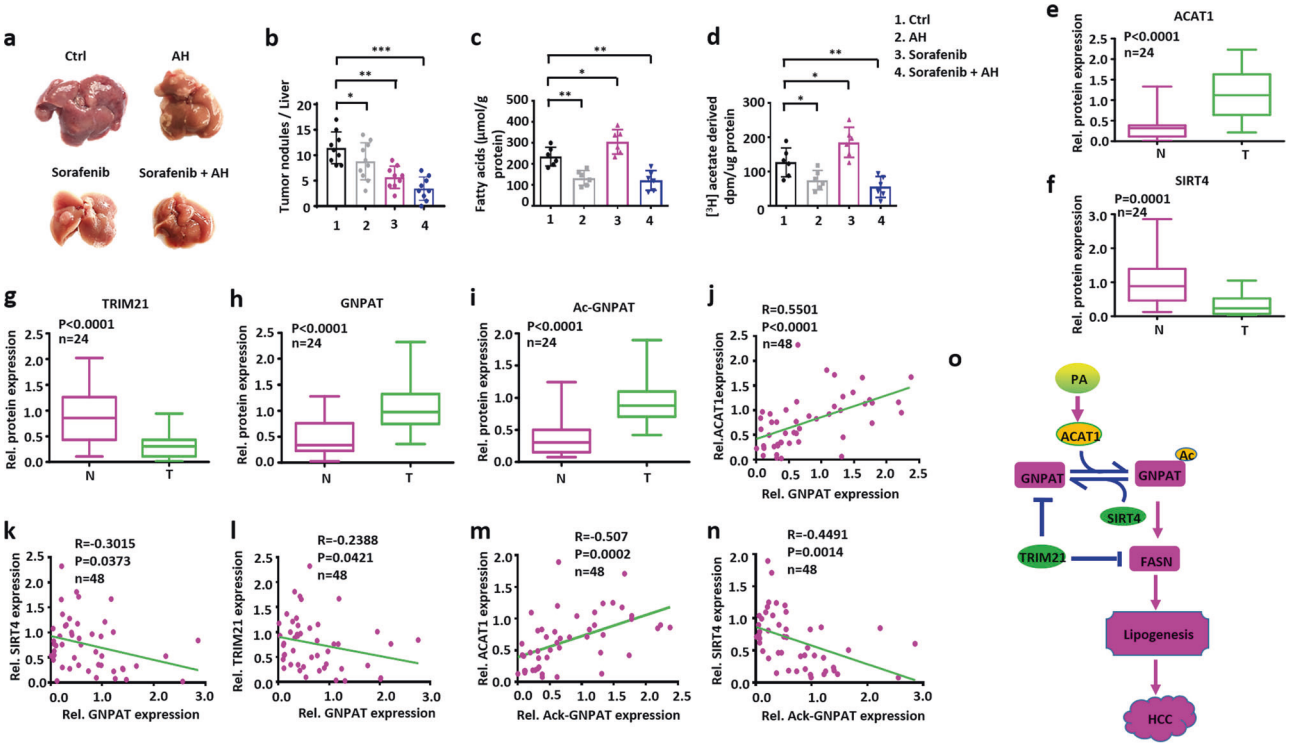

Fig. 8 Suppression of DEN/CCl_4-induced hepatocarcinogenesis by combination of sorafenib and ACAT1 inhibitor in mice. a With DEN/CCl_4-induced HCC, intraperitoneal injection with PBS (control group), sorafenib (30 mg/kg), AH (50 mg/kg), or sorafenib (30 mg/kg) with AH (50 mg/kg) for each groups three times every week after 4 months mice were born ($n = 10$). Liver images extracted from the indicated mice. Tumor nodules (**b**), fatty acids (**c**), and lipogenesis (**d**) levels from (**a**). **e–i** Relative protein levels in normal liver and HCC tissues from HCC patient samples. **j–n** Correlation of different protein levels in HCC tissues. Each point is an individual sample. *r*, Spearman correlation coefficient. Significance was performed using Wilcoxon signed rank test. The horizontal lines in the box plots represent the median, the boxes represent the interquartile range, and the whiskers represent the minimal and maximal values. **o** Schematic diagram. ACAT1 acetylates GNPAT, which represses TRIM21-mediated ubiquitination and degradation of GNPAT and FASN. GNPAT stabilizes FASN to facilitate lipid metabolism and HCC development.

Aberrant lipid metabolism is closely associated with HCC progression [26]. It has been indicated that palmitate signaling as well as stearoyl-coa desaturase activity was significantly correlated with aggressive HCC with combination of gene expression and metabolic profiling analyses from 386 HCC patients [27]. This also confirmed our results that PA plays a critical role in HCC development. Another study reported that metabolic dysregulation of lipids in hepatocytes weakened the hepatic immune surveillance and facilitated hepatocarcinogenesis by reactive oxygen species-mediated depletion of $CD4^+$ T lymphocyte [28]. Moreover, the posttranslational modifications of lipid enzymes take important part in tumorigenesis. For example, Sin1 phosphorylation by S6K dissociated Sin1 from mTORC2 and inhibited tumorigenesis [29], while GβL deubiquitination by OTUD7B facilitated mTORC2 integrity and favored tumor growth antagonized by TRAF2 ubiquitination [30]. In our report, we discovered that GNPAT was acetylated by ACAT1 at K128 and dissociated SIRT4 through deacetylation, promoting GNPAT dimerization, FAs synthesis, and subsequent tumorigenesis.

TRIM21 contains a RING finger domain which exerts E3 ligase activity [31]. Several substrates have been reported. DDX41 was degraded by TRIM21 through K48-linked ubiquitination and negative regulated innate immune response to intracellular dsDNA [32]. TRIM21 ubiquitylated P62 via K63-linked ubiquitin, preventing P62 dimerization, and sequestration [33]. In this study, we demonstrated that GNPAT acetylation repressed TRIM21-mediated GNPAT and FASN degradation, thus promoting lipid synthesis and tumorigenesis.

Last but not least, we conducted combination therapy with ACAT1 inhibitor and sorafenib firstly in the xenograft and HCC model. Significantly, combination of AH with sorafenib severely attenuated tumor growth, nearly none of the tumors seen within 7 months. Conventionally, HCC can be treated with surgical resection, liver transplantation, liver directed therapy, and systemic therapy [23]. However, only 15% patients are eligible for curative treatments since a majority of patients present with advanced disease. Sorafenib is still the only FDA approved systemic therapy for advanced HCC although it has limited efficacy [34]. And

targeting metabolic regulation of HCC is then actively performed [25]. Sorafenib toxicity was effectively enhanced by the glycolytic inhibitor 2-deoxy-glucose [35]. In our assay, synergy with AH, the effect of sorafenib was enormously strengthened. Of course, more pharmacology assay and clinical tests should be implemented in the next steps.

To sum up, we demonstrated a new mechanism that ACAT1 acetylated while SIRT4 deacetylated GNPAT at K128 under PA induction. GNPAT acetylation suppressed TRIM21-mediated degradation of GNPAT and FASN, promoting GNPAT dimerization, lipid metabolism, and HCC progression. We discovered that combination of ACAT1 inhibitor with sorafenib offered a potential target in HCC therapy.

Material and methods

Reagents, vectors, cell culture, and stable cell lines

Palmitic acid (P0500), SA (S4751), CHX (R750107), glutaraldehyde (G7651), proteasome inhibitor MG132 (M8699), and autophagy inhibitor 3-methyladenine (3-MA) (M9281) were purchased from Sigma-Aldrich. NAM (HY-B0150), TSA (HY-15144) were from Med Chem Express (MCE), and AH (S2614) and sorafenib (S7397) were purchased from Selleck. Anti-HA and anti-FLAG affinity agarose beads were purchased from Selleck (Houston, USA). Antibodies used in this study are listed in Supplementary Table S1.

The open reading frame of human GNPAT, ACAT1, SIRT4, TRIM21 were amplified and cloned into pHAGE-CMV-MCS-PGK-3 × Flag and pCMV-HA vectors. Mutations in the ubiquitin and GNPAT cDNA sequences were generated by overlap extension PCR. Human GNPAT, ACAT1, SIRT4, FASN, and TRIM21 shRNA vectors were obtained from GENECHEM (Shanghai, China). AAV vector was obtained from Yan Wang (College of Life Science, Wuhan University). Primers used in this study are listed in Supplementary Table S2. Transfection and the establishment of stable cell lines were performed as previously described [36].

Human embryonic kidney HEK293 cells and human liver tumor-derived cell lines HepG2, Hep3B, were cultured as previously described [36]. All cells, regularly authenticated by short tandem repeat analysis and tested for absence of *Mycoplasma* contamination, were used within five passages after thawing and cultured as previously described [36].

Clinical human HCC tissues

HCC samples were used as previously described [36]. Written-informed consent was obtained at the Union Hospital in Wuhan, China. The diagnoses of all samples were confirmed by histological review.

Co-immunoprecipitation and immunobloting

Transfected cells were lysed in 1 ml lysis buffer [20 mM Tris (pH 7.4), 300 mM NaCl, 1% Triton, 1 mM EDTA, 10 mg/ml aprotinin, 10 mg/ml leupeptin, and 1 mM PMSF]. Sepharose beads were washed three times with 1 ml lysis buffer containing 150 mM NaCl. Co-IP and immunoblot analysis was performed as described elsewhere [37].

Mass spectrometry analysis

HEK293T cells were transfected with Flag-GNPAT in the presence and absence of PA induction. Then cells were lysed and immunoprecipitated with anti-Flag antibody conjugated to agarose. After SDS-PAGE and Coomassie Blue staining of the immunoprecipitate, whole bands were excised, subjected to in-gel trypsin digestion and dried. The composition of protein was analyzed by MS according to the protocols described previously [17]. The volcano plot was drawed by the Software GraphPad Prism 7.

In vivo ubiquitination assay

HEK293 cells were infected or transfected with the indicated lentiviruses or specified plasmids followed by treatment with 20 μM MG132 for 6 h, washes with PBS, and lysis in RIPA buffer (50 mM Tris-HCl, pH 7.4,150 mM NaCl, 1 mM EDTA, 5 mM EGTA, 1% Nonidet P-40, 0.1% sodium deoxycholate, 10 μg/ml aprotinin, 10 μg/ml leupeptin, and 1 mM phenylmethylsulfonyl fluoride). Immunoprecipitation analysis was performed as described [17]. The samples were boiled for 10 min in SDS-PAGE sample buffer and analyzed by immunoblot with the indicated antibodies.

Metabolic assays

Serum TG levels were measured using the Infinity TGs Reagent (Thermo Scientific). Cellular nonesterified fatty acids (NEFA) levels were determined with a commercially available ELISA kit (AO42-2, Jiancheng Bio., Nanjing, China) according to the manufacturer's instruction.

Isotope experiment was performed as previously described [38]. Briefly, ^{3}H-acetic acid (1.59 Ci/mmol, Perkin Elmer, 37 KBq/ml) was added to the wells and incubated at 37 °C overnight. Then cells were disrupted with lysis buffer (100 mM Tris-HCl pH 7.5, 150 mM NaCl, 2% SDS, 10% glycerol, 12.5 mM EDTA, 1% Triton X-100 and 0.5% NP-40) and incubated at 37 °C for 30 min. Organic extraction was performed in chloroform following the protocol of Bligh and Dyer [39] and lipid-soluble products were

measured by scintillation counting (Tri-Carb 2910 TR, Perkin Elmer).

FASN activity assay

FASN enzyme activity was determined using a previously described assay [40]. In brief, cells were washed in PBS and lysed at 4 °C using scrapers in 0.1 M KPO_4 buffer (pH 7.0) containing 8% sucrose, 1 mM EDTA (pH 8.0), and 20 mM β-ME(Sigma). Lysates were centrifuged at 10,000 rpm for 10 min at 4 °C and the supernatant was mixed with assay buffer (250 mM KPO_4 buffer [pH 7], 2.5 mM EDTA, 2.5 mM DTT, 0.5 mM NADPH, 0.2 mM acetyl-CoA). The rate of NADPH oxidation was monitored at 340 nm. The substrate-dependent rate was determined by subtracting the NADPH oxidation rate from the rate measured after adding 10 µl of 1 mM malonyl-CoA (Sigma). Protein concentration of cell lysates was determined using the Bradford reagent (BioRad) and enzyme activity levels were normalized to protein amount.

Animal studies

All animal studies were approved by the Animal Care Committee of Wuhan University. For xenograft experiments, 4-week-old male BALB/c nude mice were purchased from Model Animal Research Center (Nanjing, China) and maintained in microisolator cages.

For drug treatment with xenograft mice, 5×10^6 HepG2 or Hep3B cells were injected subcutaneously to the mice ($n = 5$ per group). After 10 days, AH (50 mg/kg) or sorafenib (30 mg/kg) or combination of AH (50 mg/kg) with sorafenib (30 mg/kg) were injected to mice intraperitoneally once every other day from tumor inoculation and kept on receiving the drug until the experimental endpoint.

For the DEN/CCl_4-induced HCC, C57/B6 mice were intraperitoneally administrated 25 mg/kg of DEN (Sigma) on Day 15 of life. Following this, CCl_4 (Sigma) was then injected weekly for 12 weeks ($n = 10$ per group). Concentrated AAV-containing Acat1 shRNAs were injected by tail vein. After 30 weeks, mice were sacrificed for analysis.

For the drug treatment in DEN/CCl_4-induced HCC, it included intraperitoneal injection with phosphate-buffered saline (control group) or sorafenib at a dose of 30 mg/kg (in phosphate-buffered saline/1% Tween 80; MGH Pharmacy), the ACAT1 inhibitor AH (50 mg/kg) or sorafenib (30 mg/kg) with AH (50 mg/kg) together three times every week for each groups 4 months after mice were born.

Bioinformatics and statistics

ACAT1 protein expression data in different cancers were downloaded from the data portal (https://www.proteinatlas.org). HCC samples were assigned to two groups based on gene expression level using the minimum p value approach. Experimental data were analyzed using the unpaired, two-tailed Student's t test, Wilcoxon signed rank test, or Mann–Whitney U-test and the correlation was analyzed using a Spearman rank correlation test. Other statistical significance ($p < 0.05$) was assessed by the Student's t test. Data were presented as the mean ± SD.

Acknowledgements We thank Profs Qunying Lei (Fudan University, Shanghai) for the SIRT family vectors and FASN plasmid, Yan Wang (Wuhan University, Wuhan, China) for the AAV8 vector, Ping Wang (East China Normal University, Shanghai, China) for pcDNA3.1 (+)-5′flag Luc vector and Jinxiang Zhang (Wuhan Union Hospital, Wuahn, China) for providing the HCC samples. This work was supported by grants from the National Nature Science Foundation of China (81772609, 81902843), Medical Science Advancement Program (Basic Medical Sciences) of Wuhan University (TFJC2018005), and China Postdoctoral Science Foundation (2019T120681, 2019M652702).

Compliance with ethical standards

Conflict of interest The authors declare that they have no conflict of interest.

Publisher's note Springer Nature remains neutral with regard to jurisdictional claims in published maps and institutional affiliations.

References

1. Menendez JA, Lupu R. Fatty acid synthase and the lipogenic phenotype in cancer pathogenesis. Nat Rev Cancer. 2007;7:763–77.
2. Souchek JJ, Davis AL, Hill TK, Holmes MB, Qi B, Singh PK, et al. Combination treatment with orlistat-containing nanoparticles and taxanes is synergistic and enhances microtubule stability in taxane-resistant prostate cancer cells. Mol Cancer Ther. 2017;16:1819–30.
3. Alo PL, Amini M, Piro F, Pizzuti L, Sebastiani V, Botti C, et al. Immunohistochemical expression and prognostic significance of fatty acid synthase in pancreatic carcinoma. Anticancer Res. 2007;27:2523–7.
4. Gonzalez-Guerrico AM, Espinoza I, Schroeder B, Park CH, Kvp CM, Khurana A, et al. Suppression of endogenous lipogenesis induces reversion of the malignant phenotype and normalized differentiation in breast cancer. Oncotarget. 2016;7:71151–68.
5. Zaytseva YY, Harris JW, Mitov MI, Kim JT, Butterfield DA, Lee EY, et al. Increased expression of fatty acid synthase provides a survival advantage to colorectal cancer cells via upregulation of cellular respiration. Oncotarget. 2015;6:18891–904.
6. Kuhajda FP, Jenner K, Wood FD, Hennigar RA, Jacobs LB, Dick JD, et al. Fatty acid synthesis: a potential selective target for antineoplastic therapy. Proc Natl Acad Sci USA. 1994;91:6379–83.
7. Furuta E, Pai SK, Zhan R, Bandyopadhyay S, Watabe M, Mo YY, et al. Fatty acid synthase gene is up-regulated by hypoxia via activation of Akt and sterol regulatory element binding protein-1. Cancer Res. 2008;68:1003–11.
8. Li L, Pilo GM, Li X, Cigliano A, Latte G, Che L, et al. Inactivation of fatty acid synthase impairs hepatocarcinogenesis driven by AKT in mice and humans. J Hepatol. 2016;64:333–41.

9. Graner E, Tang D, Rossi S, Baron A, Migita T, Weinstein LJ, et al. The isopeptidase USP2a regulates the stability of fatty acid synthase in prostate cancer. Cancer Cell. 2004;5:253–61.
10. Lin HP, Cheng ZL, He RY, Song L, Tian MX, Zhou LS, et al. Destabilization of fatty acid synthase by acetylation inhibits de novo lipogenesis and tumor cell growth. Cancer Res. 2016;76:6924–36.
11. Malheiro AR, da Silva TF, Brites P. Plasmalogens and fatty alcohols in rhizomelic chondrodysplasia punctata and Sjogren-Larsson syndrome. J Inherit Metab Dis. 2015;38:111–21.
12. Rodemer C, Thai TP, Brugger B, Kaercher T, Werner H, Nave KA, et al. Inactivation of ether lipid biosynthesis causes male infertility, defects in eye development and optic nerve hypoplasia in mice. Hum Mol Genet. 2003;12:1881–95.
13. Komljenovic D, Sandhoff R, Teigler A, Heid H, Just WW, Gorgas K. Disruption of blood-testis barrier dynamics in ether-lipid-deficient mice. Cell Tissue Res. 2009;337:281–99.
14. Dorninger F, Herbst R, Kravic B, Camurdanoglu BZ, Macinkovic I, Zeitler G, et al. Reduced muscle strength in ether lipid-deficient mice is accompanied by altered development and function of the neuromuscular junction. J Neurochem. 2017;143:569–83.
15. Hossain MS, Abe Y, Ali F, Youssef M, Honsho M, Fujiki Y, et al. Reduction of ether-type glycerophospholipids, plasmalogens, by NF-kappaB signal leading to microglial activation. J Neurosci. 2017;37:4074–92.
16. Facciotti F, Ramanjaneyulu GS, Lepore M, Sansano S, Cavallari M, Kistowska M, et al. Peroxisome-derived lipids are self antigens that stimulate invariant natural killer T cells in the thymus. Nat Immunol. 2012;13:474–80.
17. Gu L, Zhu Y, Lin X, Li Y, Cui K, Prochownik EV, et al. Amplification of glyceronephosphate O-acyltransferase and recruitment of USP30 stabilize DRP1 to promote hepatocarcinogenesis. Cancer Res. 2018;78:5808–19.
18. Haapalainen AM, Merilainen G, Wierenga RK. The thiolase superfamily: condensing enzymes with diverse reaction specificities. Trends Biochem Sci. 2006;31:64–71.
19. Fan J, Shan C, Kang HB, Elf S, Xie J, Tucker M, et al. Tyr phosphorylation of PDP1 toggles recruitment between ACAT1 and SIRT3 to regulate the pyruvate dehydrogenase complex. Mol Cell. 2014;53:534–48.
20. Fan J, Lin R, Xia S, Chen D, Elf SE, Liu S, et al. Tetrameric acetyl-CoA acetyltransferase 1 is important for tumor growth. Mol Cell. 2016;64:859–74.
21. O'Brien CA, Kreso A, Ryan P, Hermans KG, Gibson L, Wang Y, et al. ID1 and ID3 regulate the self-renewal capacity of human colon cancer-initiating cells through p21. Cancer Cell. 2012;21:777–92.
22. J Jin, J Liu, C Chen, Z Liu, C Jiang, H Chu, et al. The deubiquitinase USP21 maintains the stemness of mouse embryonic stem cells via stabilization of Nanog. Nat Commun. 2016;7:13594.
23. Kim DW, Talati C, Kim R. Hepatocellular carcinoma (HCC): beyond sorafenib-chemotherapy. J Gastrointest Oncol. 2017;8:256–65.
24. Ferlay J, Soerjomataram I, Dikshit R, Eser S, Mathers C, Rebelo M, et al. Cancer incidence and mortality worldwide: sources, methods and major patterns in GLOBOCAN 2012. Int J Cancer. 2015;136:E359–86.
25. Lee M, Ko H, Yun M. Cancer metabolism as a mechanism of treatment resistance and potential therapeutic target in hepatocellular carcinoma. Yonsei Med J. 2018;59:1143–9.
26. Gingold JA, Zhu D, Lee DF, Kaseb A, Chen J. Genomic profiling and metabolic homeostasis in primary liver cancers. Trends Mol Med. 2018;24:395–411.
27. Budhu A, Roessler S, Zhao X, Yu Z, Forgues M, Ji J, et al. Integrated metabolite and gene expression profiles identify lipid biomarkers associated with progression of hepatocellular carcinoma and patient outcomes. Gastroenterology. 2013;144:1066–75. e1061.
28. Ma C, Kesarwala AH, Eggert T, Medina-Echeverz J, Kleiner DE, Jin P, et al. NAFLD causes selective CD4(+) T lymphocyte loss and promotes hepatocarcinogenesis. Nature. 2016;531:253–7.
29. Liu P, Gan W, Inuzuka H, Lazorchak AS, Gao D, Arojo O, et al. Sin1 phosphorylation impairs mTORC2 complex integrity and inhibits downstream Akt signalling to suppress tumorigenesis. Nat Cell Biol. 2013;15:1340–50.
30. Wang B, Jie Z, Joo D, Ordureau A, Liu P, Gan W, et al. TRAF2 and OTUD7B govern a ubiquitin-dependent switch that regulates mTORC2 signalling. Nature. 2017;545:365–9.
31. Wei Z, Song J, Wang G, Cui X, Zheng J, Tang Y, et al. Deacetylation of serine hydroxymethyl-transferase 2 by SIRT3 promotes colorectal carcinogenesis. Nat Commun. 2018;9:4468.
32. Zhang Z, Bao M, Lu N, Weng L, Yuan B, Liu YJ. The E3 ubiquitin ligase TRIM21 negatively regulates the innate immune response to intracellular double-stranded DNA. Nat Immunol. 2013;14:172–8.
33. Pan JA, Sun Y, Jiang YP, Bott AJ, Jaber N, Dou Z, et al. TRIM21 ubiquitylates SQSTM1/p62 and suppresses protein sequestration to regulate redox homeostasis. Mol Cell. 2016;61:720–33.
34. Gong XL, Qin SK. Progress in systemic therapy of advanced hepatocellular carcinoma. World J Gastroenterol. 2016;22:6582–94.
35. Tesori V, Piscaglia AC, Samengo D, Barba M, Bernardini C, Scatena R, et al. The multikinase inhibitor sorafenib enhances glycolysis and synergizes with glycolysis blockade for cancer cell killing. Sci Rep. 2015;5:9149.
36. Han H, Sun D, Li W, Shen H, Zhu Y, Li C, et al. A c-Myc-MicroRNA functional feedback loop affects hepatocarcinogenesis. Hepatology. 2013;57:2378–89.
37. Zhu Y, Gu L, Li Y, Lin X, Shen H, Cui K, et al. miR-148a inhibits colitis and colitis-associated tumorigenesis in mice. Cell Death Differ. 2017;24:2199–209.
38. Lv L, Li D, Zhao D, Lin R, Chu Y, Zhang H, et al. Acetylation targets the M2 isoform of pyruvate kinase for degradation through chaperone-mediated autophagy and promotes tumor growth. Mol Cell. 2011;42:719–30.
39. Bligh EG, Dyer WJ. A rapid method of total lipid extraction and purification. Can J Biochem Physiol. 1959;37:911–7.
40. Knobloch M, Braun SM, Zurkirchen L, von Schoultz C, Zamboni N, Arauzo-Bravo MJ, et al. Metabolic control of adult neural stem cell activity by Fasn-dependent lipogenesis. Nature. 2013;493:226–30.